General Disclaimer

One or more of the Following Statements may affect this Document

- This document has been reproduced from the best copy furnished by the organizational source. It is being released in the interest of making available as much information as possible.

- This document may contain data, which exceeds the sheet parameters. It was furnished in this condition by the organizational source and is the best copy available.

- This document may contain tone-on-tone or color graphs, charts and/or pictures, which have been reproduced in black and white.

- This document is paginated as submitted by the original source.

- Portions of this document are not fully legible due to the historical nature of some of the material. However, it is the best reproduction available from the original submission.

RAYTHEON COMPANY
EQUIPMENT DIVISION

RAYTHEON

CAT LIDAR WIND SHEAR STUDIES

TECHNICAL REPORT

ER78-4081

1 March 1978

CONTRACT NAS8-28424

Prepared for

GEORGE C. MARSHALL SPACE FLIGHT CENTER

NASA

Huntsville, Alabama 35812

Prepared by

Roger W. Goff

RAYTHEON COMPANY
EQUIPMENT DEVELOPMENT LABORATORIES
ADVANCED DEVELOPMENT LABORATORY
ELECTRO-OPTICS DEPARTMENT
Sudbury, Massachusetts 01776

CAT LIDAR WIND SHEAR STUDIES

1. INTRODUCTION

Three major commercial aircraft accidents occurring during the past several years, and linked by the National Transportation Safety Board to wind shear, have demonstrated the serious threat this phenomenon represents to safe aircraft operations in the terminal area. These accidents were: Iberian Airlines DC10-30, Logan International Airport, December 17, 1973 (accident occurred on landing)[1]; Eastern Airlines, B727-225, JFK International Airport, June 24, 1975 (accident occurred on landing)[2]; and Continental Airlines B727-224, Stapleton Airport, August 7, 1975 (accident occurred on takeoff)[3].

Remote ground-based sensing of wind field characteristics represents a possible solution to the wind shear hazard. Ground-based equipment has the advantage over airborne equipment of (1) providing information to general aviation aircraft for which airborne wind shear avionics may be economically unfeasible and (2) alerting the pilot prior to takeoff or prior to entry into hazardous shear (on landing) thus avoiding the hazard completely or allowing a timely go-around maneuver.

CO_2 pulse Doppler LIDAR has been recognized as a viable candidate for the remote ground based detection of wind fields. As part of the CAT system improvement studies, the application of the MSFC CAT LIDAR (and improved versions of this sensor) have been examined as possible wind shear sensors.

The studies have considered the major meteorological factors producing wind shear, methods to define and classify wind shear in terms significant from an aircraft perturbation standpoint, the significance of sensor location and scan geometry on the detection and measurement of wind shear and the tradeoffs involved in sensor performance such as range/velocity resolution, update frequency and data averaging interval. This memo summarizes the study results.

2. SHEAR PRODUCING WEATHER CONDITIONS

The three most significant weather phenomena causing hazardous wind shear are thunderstorms, frontal systems and low level temperature inversions. The flow fields accompaning these phenonena are characterized in Figures 1, 2 and 3.

The gust front preceding a thunderstorm is characterized by high turbulence, strong updrafts and downdrafts and large shear producing windshifts. Moreover, the gust front can precede the storm itself by 10 or more miles.

Frontal systems are dangerous to aircraft when they are moving at speeds greater than 30 knots and have temperature differences across the front of 10°F or greater. Wind shifts occurring across and along the frontal surface produce wind shear. Normally the most severe shear from a cold front occurs just after frontal passage, conversely, the shear created by a warm front occurs just prior to passage of the front, (i.e., on the cooler side of the front in both cases). Warm fronts are normally much shallower in slope than cold fronts. This fact is discussed more completely in a later section, but essentially it results in warm front shears being encountered with a vertical change in position (approximate horizontal striation of the air mass) and cold front shear being encountered with a horizontal change in position (approximate vertical striation of the air mass).

3. WIND SHEAR DEFINITION

In general, wind shear is a change in wind velocity with position or time. Since wind shear is normally measured by instrumented towers, it is commonly given as the change in horizontal wind speed occurring over some height interval. From an aircraft performance standpoint the concern is with the change in aircraft airspeed induced by changes in the wind field occurring between points on the flight path. This is true whether the aircraft is landing, flying level or climbing out as shown in Figure 4.

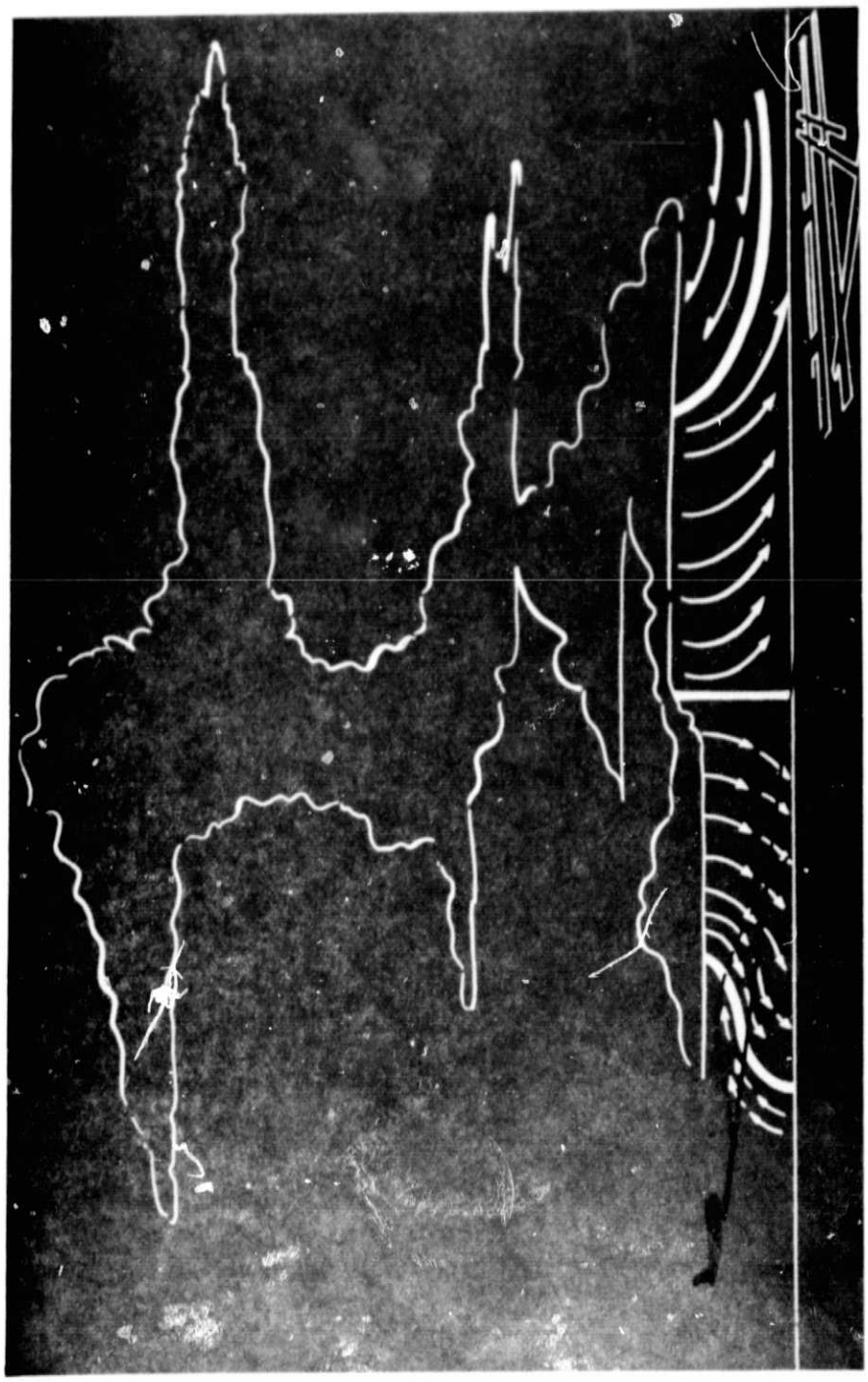

Figure 1. Typical Thunderstorm Threat.

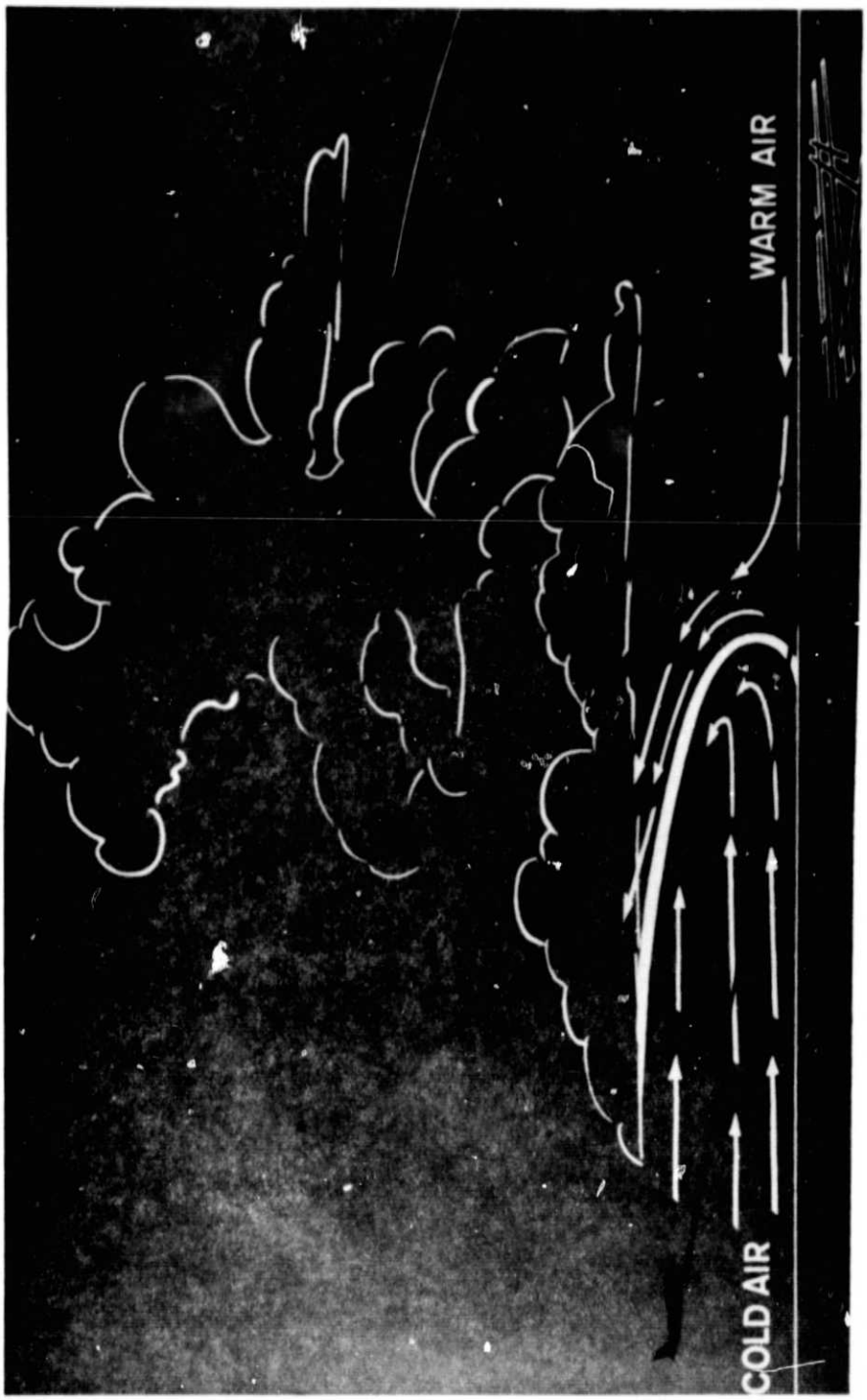

Figure 2. Typical Front Threat.

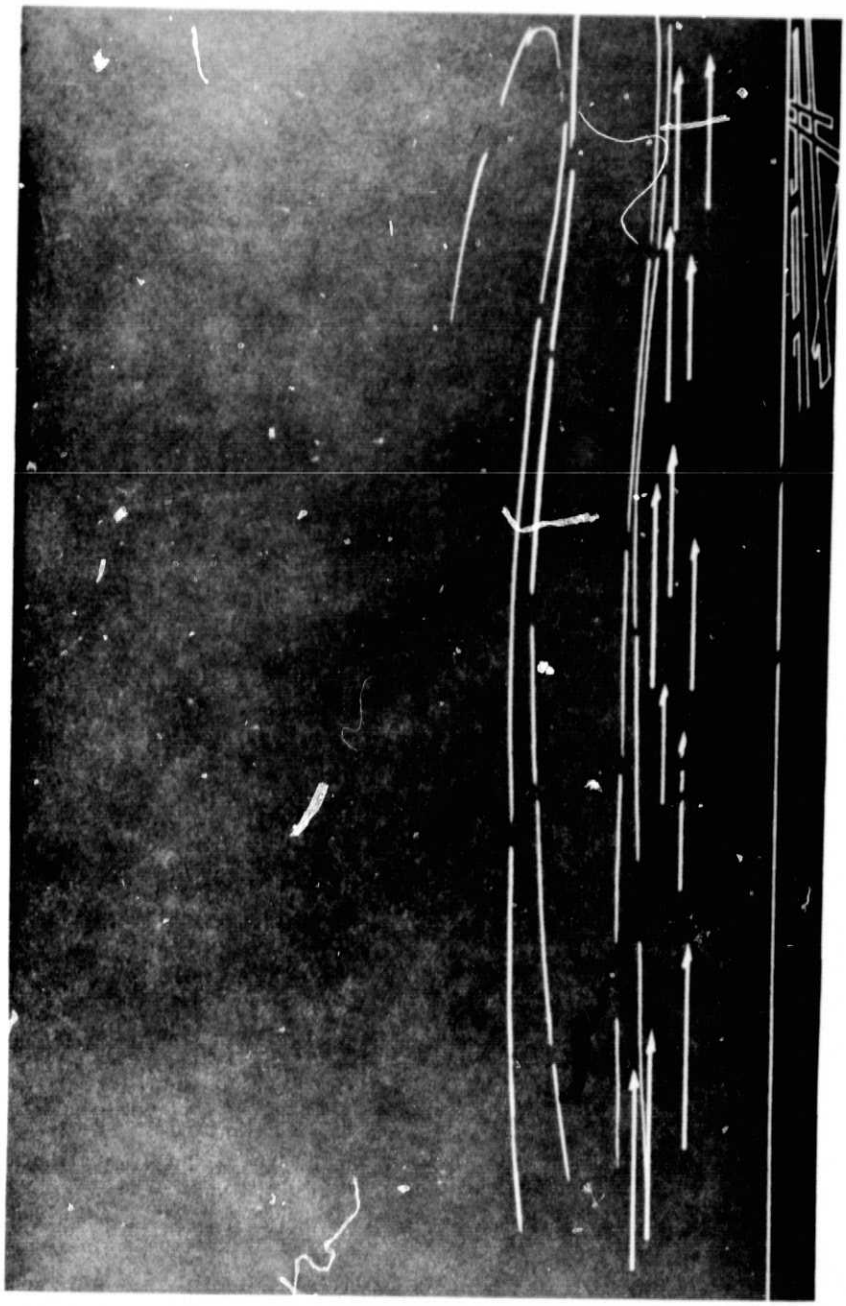

Figure 3. Typical Inversion Threat.

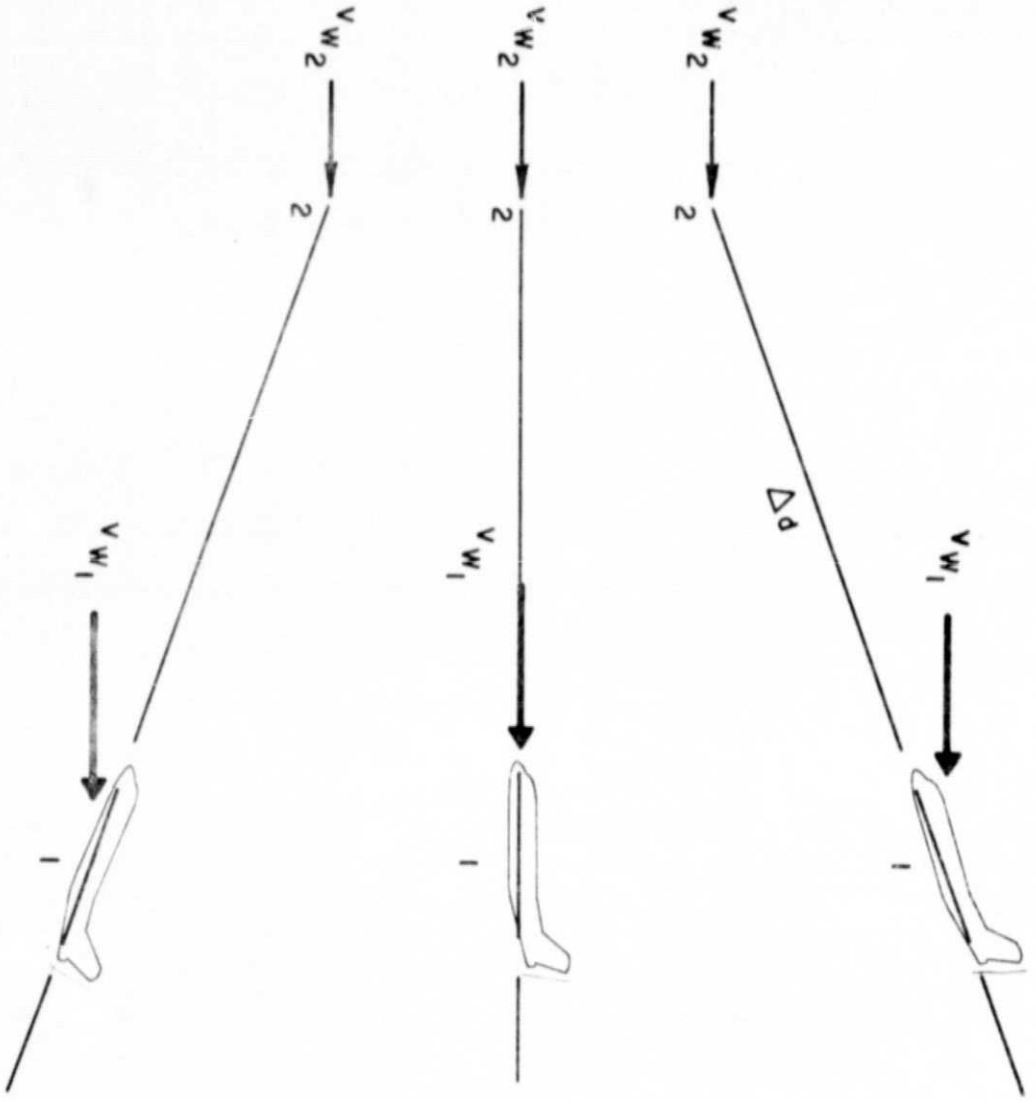

Figure 4. Aircraft Related Shear.

Compared to the component of wind along the flight path, the other components are lesser concern to the pilot since they do not directly affect airspeed. These are the cross wind component (causes lateral drift) and the vertical component (updraft/downdraft). The latter are known to be severe in conjunction with major thunderstorm activity and probably were significant in the Eastern crash at Kennedy International Airport[2].

If we assume that the aircraft in Figure 4 is trimmed for unaccelerated flight at point one, and is unaccelerated by the wind variation between points one and two; the airspeed change or wind shear between points one and two is equal to the difference between the vector wind at one and two projected along the flight path, ΔV_f. Fichtl[4] gives the following expression for ΔV_f:

$$\Delta V_f = (\Delta \bar{u} + \Delta u') \sin\gamma \cos\theta + \Delta v' \sin\gamma \sin\theta + \Delta w' \cos\gamma \qquad (1)$$

where

$$\Delta \bar{u} = \bar{u}(z_2) - \bar{u}(z_1)$$

$$\Delta u' = u'(x_2, y_2, z_2, t_2) - u'(x_1, y_1, z_1, t_1)$$

$$\Delta v' = v'(x_2, y_2, z_2, t_2) - v'(x_1, y_1, z_1, t_1)$$

$$\Delta w' = w'(x_2, y_2, z_2, t_2) - w'(x_1, y_1, z_1, t_1)$$

and $\bar{u}(z)$ = the mean wind speed at height (z)

u', v', w' are the x, y, z components of the turbulent velocity vector.

Equation (1) is the total wind change between points one and two along the aircraft's flight path. As previously mentioned, wind shear is normally expressed as the change in horizontal wind between two different heights; in the aircraft case (where the aircraft can be flying level, climbing or descending) a more suitable measure is the wind change, ΔV_f, divided by either the time of flight between points one and two or the distance along the flight path between points one and two (Δd) as shown on Figure 4. In the former case the wind shear would be the wind change (or airspeed change induced by the wind) expected per unit time, while in the latter case, the shear would be the wind change per unit distance along the flight path.

$$(WS)_t = \frac{\Delta V_f}{(t_2 - t_1)}$$

$$(WS)_d = \frac{\Delta V_f}{(d_2 - d_1)} \qquad (2)$$

For convenience of reporting, shears could be referenced to some convenient value of time or distance, e.g., 1 min. or 1000 meters,

$$\overline{(WS)}_t = \frac{\Delta V_f}{(t_2 - t_1)} \cdot 60 \text{ sec}$$

$$\overline{(WS)}_d = \frac{\Delta V_f}{(d_2 - d_1)} \cdot 1000 \text{ m} \qquad (3)$$

Equations (3) are suggested as appropriate indices for expressing wind shear magnitudes. They are particularly well suited to being measured by glide slope scanning sensors.

The above wind shear indices are compared with the ICAO standard wind shear categories in Table 1, for an aircraft landing along a

three degree glide slope at 125 kts (64.4m/sec). The ICAO wind shear categories are related to the variation of the horizontal wind (m/sec) in a 30 meter height interval.

	Wind Shear Parameter		
	Height Related	Aircraft Related	
ICAO Category	m/sec/30m alt.	$(\overline{WS})_t$, m/sec/60 sec	$(\overline{WS})_d$, m/sec/1000 m range
Light	0 - 2.5	0 - 16.9	0 - 4.4
Moderate	2.5 - 4.5	16.9 - 30.4	4.4 - 7.9
Strong	4.5 - 6.0	30.4 - 40.6	7.9 - 10.5
Severe	>6.0	>40.6	>10.5

Table 1. Indices for Wind Shear Severity.

Describing shear in terms of the wind change that occurs over some distance along the flight path or over some elapsed time appears more suitable than using the ICAO standard approach. The shear so described relates directly to aircraft performance changes and is readily obtained from the output of a glide slope or quasi glide slope sensor. The method is not as compatible with vertical probe (VAD) type sensors, that generate information similar to tower data. The glide path indices can be computed from vertical probe data provided horizontal homogeneity of the wind field is assumed.

4. AIRCRAFT PERTURBATIONS DUE TO SHEAR

In order to assess aircraft glide slope excursions due to wind shear without resorting to numerical integration of the aircraft equations of motion a simplified model for computing these excursions was derived.

The algorithm, which gives reasonable predictions for short duration flight (10-15 sec maximum) in uniform shear, assumes that

the headwind/tailwind varies linearly over some altitude or equivalent glide slope distance.

The perturbations are computed along (s) and normal (n) to the glide slope as shown in Figure 5. The aircraft is flying at a velocity of V_{ac} and is assumed to be trimmed for unaccelerated flight along the glide slope. The perturbational acceleration ($\ddot{n}$) in a direction normal to the glide slope experienced by an aircraft in wind shear relative to an aircraft experiencing zero shear is given by:

$$\ddot{n} = \left(\frac{g}{w}\right) \frac{1}{2} C_L \rho S \left(V^2_{a_{SHEAR}} - V^2_{a_{NO\ SHEAR}}\right), \qquad (4)$$

where g = the gravitational acceleration
w = the aircraft weight
C_L = the aircraft lift coefficient
ρ = the atmospheric density
S = the aircraft reference area

$V_{a_{SHEAR}}$ = the aircraft airspeed in a wind shear environment

$V_{a_{NO\ SHEAR}}$ = the aircraft airspeed in a zero wind shear environment

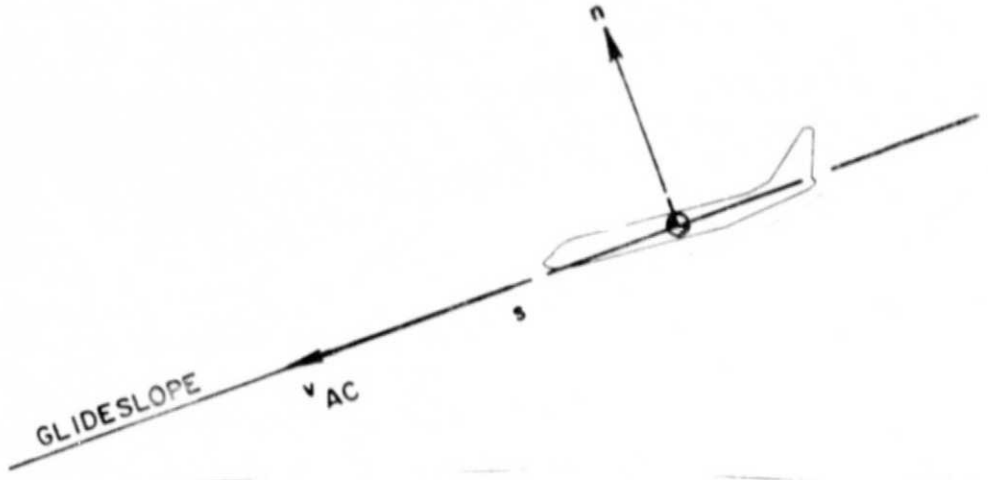

Figure 5. Perturbation Model Geometry.

In a wind shear that varies linearly with altitude or distance along a shallow glide slope (typically -3°), the aircraft airspeed variation can be written:

$$V_{a_S} = V_{a_{NS}} - V_w' \, t \tag{5}$$

where V_w' is the rate of change of tailwind speed with time (dV_w/dt)

Substituting Equation 5 into 4 and simplifying

$$\ddot{n} = g\left(\frac{L}{W}\right)\left[-2\,\frac{V_w'}{V_{a_{NS}}}\,t + \left(\frac{V_w'}{V_{a_{NS}}}\,t\right)^2\right] \tag{6}$$

integrating

$$n = g\left(\frac{L}{W}\right)\left[-\frac{1}{3}\left(\frac{V_w'}{V_{a_{NS}}}\right)t^3 + \frac{1}{12}\left(\frac{V_w'}{V_{a_{NS}}}\right)^2 t^4\right] \tag{7}$$

For an aircraft trimmed for landing $L/W \simeq 1$ and since the second term in brackets is $<<$ the first term, Equation (7) can be simplified to

$$n = g\left[-\frac{1}{3}\left(\frac{V_w'}{V_{a_{NS}}}\right)t^3\right] \tag{8}$$

Furthermore, since $V_w' = \dfrac{dV_w}{dt} = \dfrac{dV_w}{ds} \cdot \dfrac{ds}{dt}$, and

$$\frac{ds}{dt} \simeq V_{a_{NS}}$$

$$V_w' = \frac{dV_w}{ds} \cdot V_{a_{NS}} \simeq \frac{\Delta V_w}{\Delta s} \cdot V_{a_{NS}} \tag{9}$$

Substituting Equation (9) into (8)

$$n \simeq g\left[-\frac{1}{3}\left(\frac{\Delta V_w}{\Delta s}\right)t^3\right] \quad , \quad t < 10\text{-}15 \text{ sec} \qquad (10)$$

Equation (10) is an approximate expression for the short term departure of an aircraft above or below the glide slope, for a linear change in tailwind, expressed as the change in tailwind (ΔV_w) over some distance (Δs) along the glide slope. For the sign convention assumed, ΔV_w, is positive for an increase in tailwind (decrease in headwind) and vice versa. Equation (10) has been used for assessing critical glide slope departures due to shear.

5. CO_2 DOPPLER LIDAR DEPLOYMENT ALTERNATIVES

CO_2 Doppler LIDAR systems for use at airports for wind shear detection can be sub-divided into short and long range applications. Short range applications include the operation of CW Doppler LIDAR in a VAD mode. For long range applications pulse-Doppler systems are applicable. Pulsed Doppler LIDARS (of primary concern in this memo) can be further sub-divided into glide slope or quasi glide slope wind scanning systems and central airport wind shear surveillance systems. A surveillance sensor would present data similar to a weather radar, but presenting wind Doppler information. Shear surveillance data would be obtained by scanning continuously in azimuth or over a selected azimuth sector at a shallow elevation angle.

6. SYSTEM MEASUREMENT TRADEOFFS

Involved in the design of a wind shear system are questions concerned with data averaging and (for pulsed systems) the choice of a pulse length which gives a reasonable compromise between system velocity and range resolution.

A hypothetical glide slope wind measuring system might consist of an array of anemometers mounted on towers spaced evenly along the aircraft flight path. Neglecting for the moment the impracticality of such a system, data collected from the anemometers would represent

an average based upon some time interval. The time interval would be chosen as long as possible in the interest of smoothing noise, but not so long as to disguise the minimum size wind variations of interest. Also, the anemometer spacing would be chosen to include wind variation wavelengths that significantly affect the aircraft flight path.

The tradeoffs for a LIDAR system scanning the glide slope are concerned with similar questions, choices of data integration and averaging intervals as well as velocity and range resolution. A LIDAR system looking up the glide slope would be required to resolve shear gusts (changes in wind along the aircraft path) that result in significant aircraft departures from the glide slope.

Although incomplete at this time, some data does exist on the history of maximum wind shears observed at particular stations. Page 319 of Reference 5 contains applicable data including the effects of averaging interval on the maximum recorded shear. This data presented in Figure 6 was assumed to be typical of what might be observed at an airport.

For each interval the average shear listed can be interpreted as the maximum average shear over the interval. The product of this maximum average shear and the averaging interval (Δt), $\left(\frac{dV_w}{dh}\right)$. Δt, can be considered the maximum wind shear "gust impulse" that an aircraft would experience in that time interval.

This data can be easily converted to the expected air speed change if a homogeneous atmosphere is assumed and the glide slope and aircraft speed are known. Furthermore, through the simplified equation for predicting aircraft perturbations in shear (Equation 10) the maximum aircraft glide slope departure as a function of averaging interval can be determined. A minimum significant averaging interval can then be defined.

Figure 7 presents the maximum glide slope departure (from Equation 10), obtained as a function of averaging interval for the worst shear data of Figure 6.

An allowable aircraft glide slope departure was assumed to be a 1/2 scale deflection of the glide slope needle at a distance from touchdown of 1/2 nmi. This corresponds to a 19 ft. glide slope departure

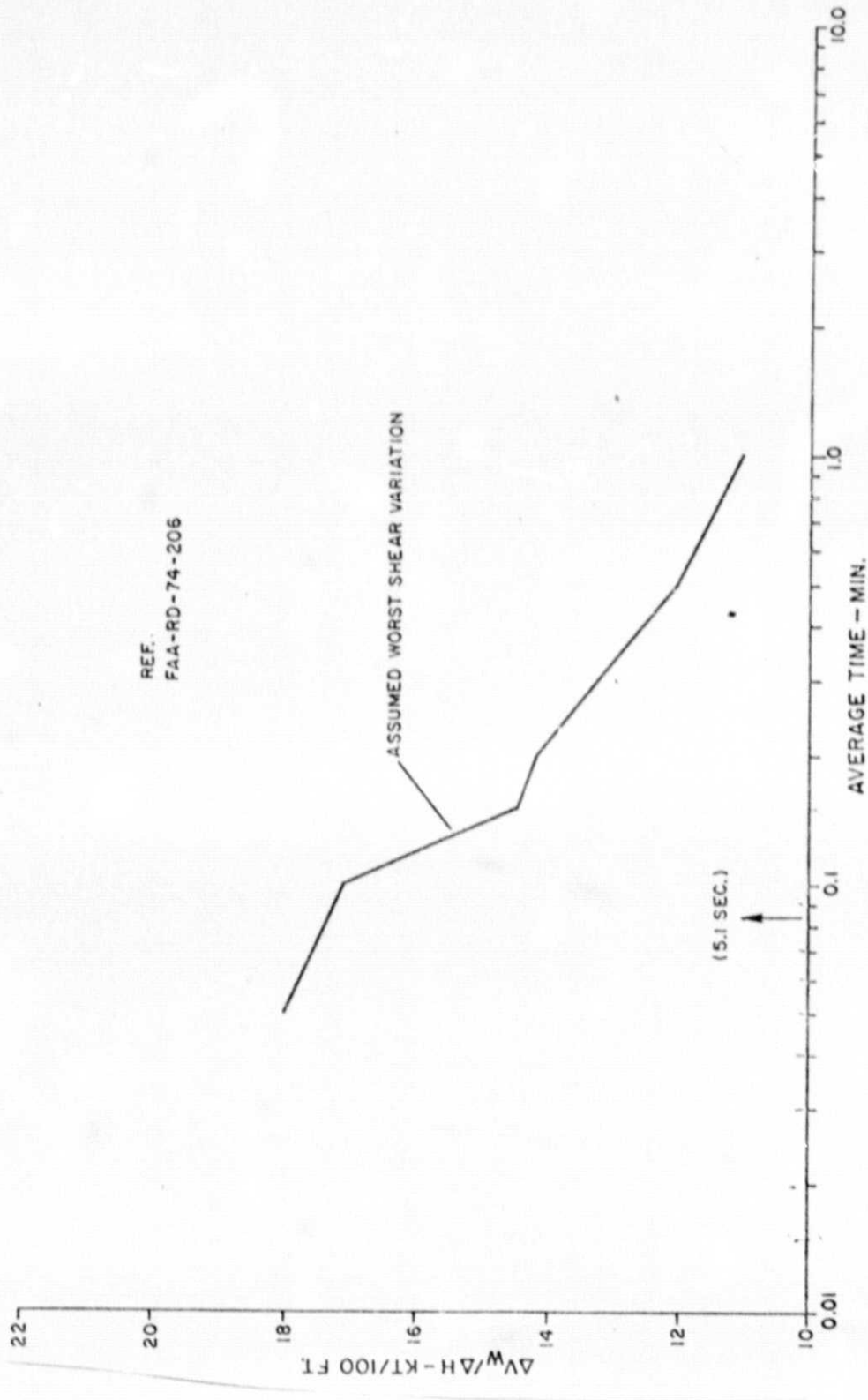

Figure 6. Maximum Shear vs. Averaging Time.

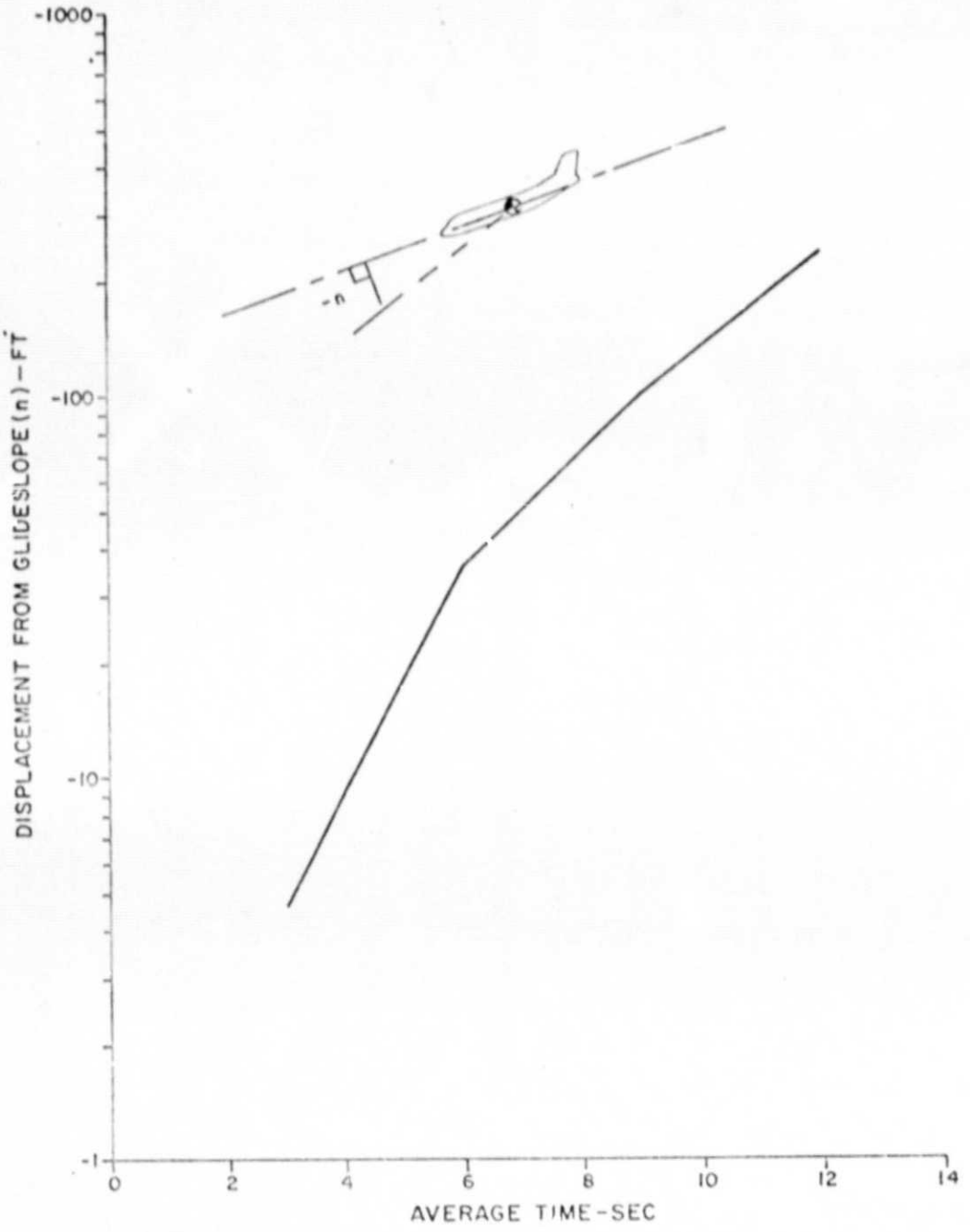

Figure 7. Maximum Glide Slope Departure vs. Averaging Time.

or an averaging time of 5.1 seconds based on the data of Figure 7. This means that if an aircraft flying at 125 knots encounters the maximum average shear measured in the data of Figure 6 for a 5.1 second interval, a glide slope departure of 19.1 feet will occur. If the data is averaged over an interval greater than 5.1 seconds, wind changes will be excluded that can produce departures of greater than 19 feet. If data is averaged over an interval less than 5.1 seconds wind changes will be measured to a resolution greater than the assumptions require.

In 5.1 seconds at 125 knots, an aircraft will travel 328 meters. From Figure 6 the sensor must be capable of resolving a shear of 17.4 ft/sec/100 ft (altitude). Along a glide slope inclined at 3 degrees this amounts to a wind shear of 3 m/sec in 328 meters (9.1 m/sec/1000 meters).

At the CO_2 wavelength, a 2 μsec pulse length corresponds to a range resolution of 300 m and a velocity resolution of 2.65 m/sec. Therefore, a pulse Doppler LIDAR (including the present CAT system) operating at a pulse length of 2 μsec is reasonably compatible with the required resolution requirements. Processing to improve velocity resolution over the unprocessed 2.65 m/sec value would be desirable to improve accuracy. Using a system with a shorter pulse and matched filters would result in reduced signal-to-noise ratios as a result of the smaller sample volume. It is desirable to utilize the longest pulse consistent with the laser technology and the resolution desired. It happens in this application that the technology and the system requirements resolution coincide at approximately 2 μsec.

To summarize, a preliminary analysis has shown that a CO_2 pulse Doppler LIDAR operating in a glide slope mode must be capable of resolving wind gust impulses of approximately 3 m/sec over a range cell of 300 meter in order to detect wind changes causing glide slope departures equivalent to a 1/2 scale deflection of the glide slope instrument at a distance 1/2 nmi from touchdown. Data may be averaged for up to 5 seconds and still identify wind shear gusts to the required resolution.

No attempt was made to examine the processing required to extract the change in wind or Doppler velocity within a resolution cell. One

method would be to difference the mean Doppler from adjacent resolution cells. Likewise, within a resolution cell, it may be possible to extract the change in Doppler based on knowledge of the mean and higher data moments.

Useful information concerning the applications and requirements for a CO_2 pulse Doppler LIDAR wind shear sensor can be obtained if the Doppler returns from realistic wind fields are examined as a function of system parameters such as sensor location, scan geometry, scan update interval, etc.

To provide this insight, the returns measured by a sensor situated at the touchdown location and looking up the glide slope, as well as a sensor displaced from this location, but still looking in the general glide slope direction have been examined.

Two wind fields were selected. The first, shown in Figure 8, is representative of the thunderstorm gust front outflow model used by the FAA in studies of aircraft perturbations due to shear. This wind field is horizontally homogeneous and stationary and, therefore, the wind characteristics are independent of horizontal position (x,y) and time and vary only with altitude (z). As pointed out by Fichtl[4] these conditions are rarely realized in the atmospheric boundary layer because of significant variations in surface roughness and heat-transfer properties in the horizontal.

The second model wind field was selected from Reference (6) and represents the actual wind field measured in a plane defined by an instrumented tower and the mean wind velocity during the passage of a thunderstorm front. The temporal variation of the three components of wind measured at several heights along the tower were recorded and smoothed to produce two-dimensional contour plots of the 3-components of velocity, temperature and the streamline geometry. The temporal data was converted to spatial data using Taylor's hypothesis. This wind field data (case G of the reference) is shown in Figure 9.

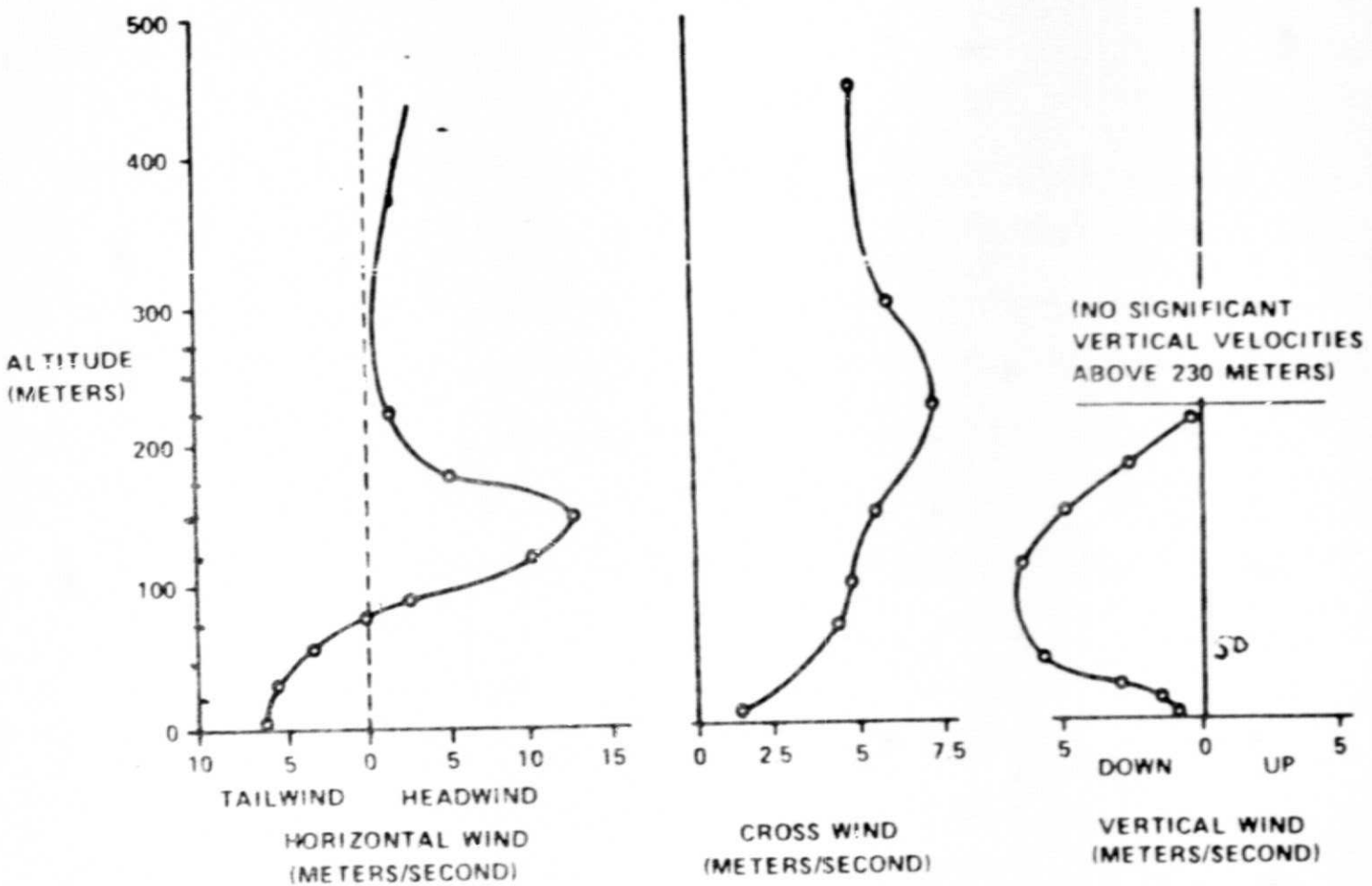

Figure 8. Thunderstorm Cold Air Outflow (Gust Front).

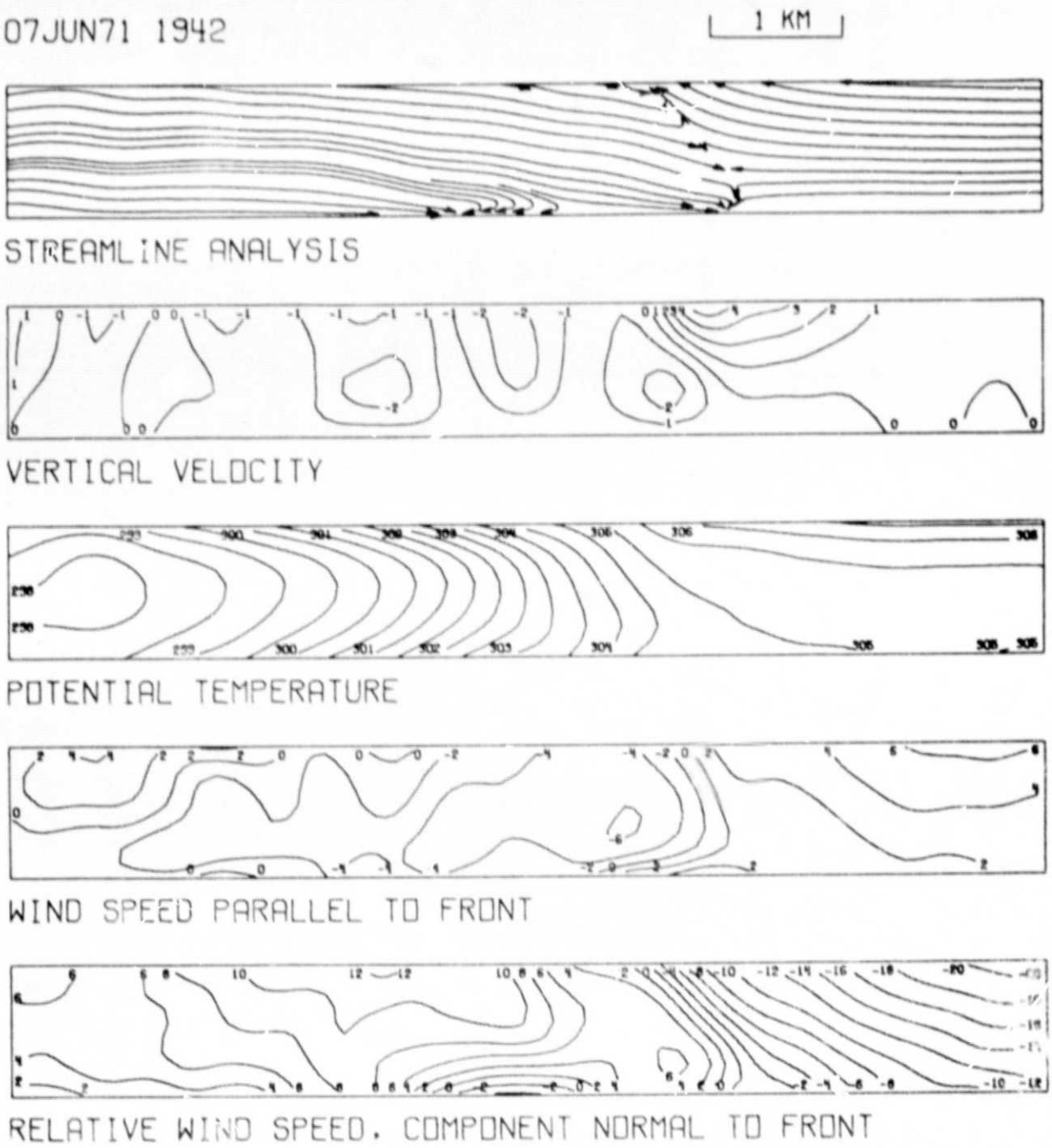

Figure 9. Temperature and Wind Stream Characteristics Measured During Frontal Passage.

The two model wind fields represented in Figures 8 and 9 were used to analyze the Doppler velocity measured along the sensor line-of-sight (LOS) as it was directed up the glide slope, and also as the LOS was directed in the general glide slope direction, but with the sensor displaced from the touchdown location in the down runway direction. Doppler data was also examined for both sensor locations when the beam was scanned laterally (windfield of Figure 8 only). For simplicity the sensor was kept aligned with the runway centerline in all cases. The effects of laterally offsetting the sensor from the runway centerline by an amount meeting FAA installation standards are expected to be small.

Figure 10 was developed from the data of Figure 9 assuming a glide slope angle of 3 degrees and an aircraft speed of 125 knots. The figure compares the Doppler experienced by the aircraft as it flies down the glide slope (heavy curve) with that measured by a glideslope sensor located at the touchdown point and directed up the glide slope. The four lighter curves represent the Doppler observed by the sensor at zero time when the aircraft is at a distance of 7.5 kilometers from touchdown and at times of 1, 2 and 3 minutes.

For the gust front examined, the tailwind observed by the aircraft begins at a distance of 7500 m with a value of approximately 18 m/sec, increases slightly at first to a value of 22 m/sec before dropping sharply to a tailwind of 4 m/sec at touchdown. This variation in tailwind causes an initial drop in airspeed (increase in tailwind), which would result in a drop below the glide slope, followed by an increase in airspeed (decrease in tailwind) causing a performance increase or a rise above the glide slope.

The magnitude of the shear experienced is shown by the slope of the shear magnitude scale in the lower right hand portion of the figure. As shown, the performance increasing change in tail wind would be classified as a severe shear by ICAO standards and would obviously precipitate a go-around maneuver.

The front in this particular case if moving at a speed of 11.8 m/sec past the sensor. The aircraft time of flight from a range of 7500 m to touchdown is 113 seconds. At zero time the doppler observed by the glide slope sensor matches the aircraft doppler for the first few thousand meters beginning at zero flight time. Similarly, at 1 minute the sensor observed doppler is similar to the aircraft experienced doppler near touchdown. At 2 minutes the front is beginning to move past the sensor and at 3 minutes the sharp wind change associated with the front has moved past the sensor.

Several points can be made based on the data of Figure 10. First, a glide slope sensor with zero minimum range capability adequately predicts the airspeed charges experienced by an aircraft flying the same slope in spite of temporal differences. Secondly, a surveillance sensor scanning 360° in azimuth and updating on the order of once each minute would adequately track this particular front (frontal speed 11.8 m/sec) as it moved through the airport area.

Because of the finite minimum range time of the CAT and other CO_2 pulse Doppler LIDARS (approximately 15 μs for CAT), the second situation examined assumed the sensor to be displaced down the runway by a distance of 2000 meters. The data for this case is shown in Figure 11.

The sensor LOS was directed to pass through the aircraft glide slope at a point immediately above the middle marker as shown in the sketch in the lower right hand corner of the figure. Note that range is referenced to the touchdown location. Again the sensor adequately predicts the airspeed changes along the glide slope. It should be observed that one reason the wind field is adequately measured by the displaced sensor is that the wind field is vertically striated (see lower curve of Figure 9). For a horizontally striated wind field, as represented by the wind field of Figure 8, this is not true.

The horizontally homogeneous wind field depicted in Figure 8 was used to examine the Doppler characteristics measured by a glide slope sensor located at touchdown and also displaced from touchdown

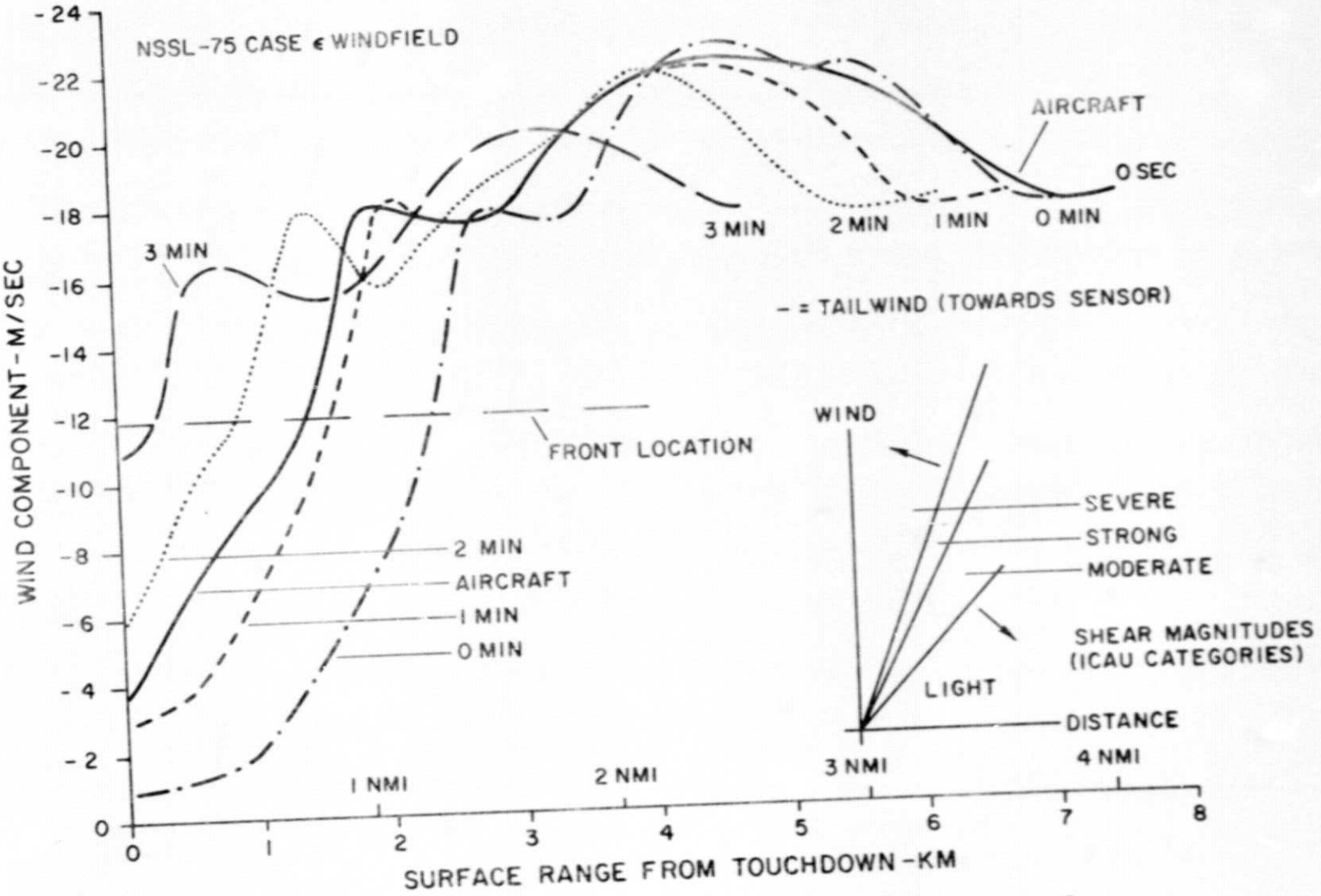

Figure 10. Comparison of Aircraft Experienced Wind and Glide Slope Sensor Measurements

RAYTHEON COMPANY
EQUIPMENT DIVISION
RAYTHEON

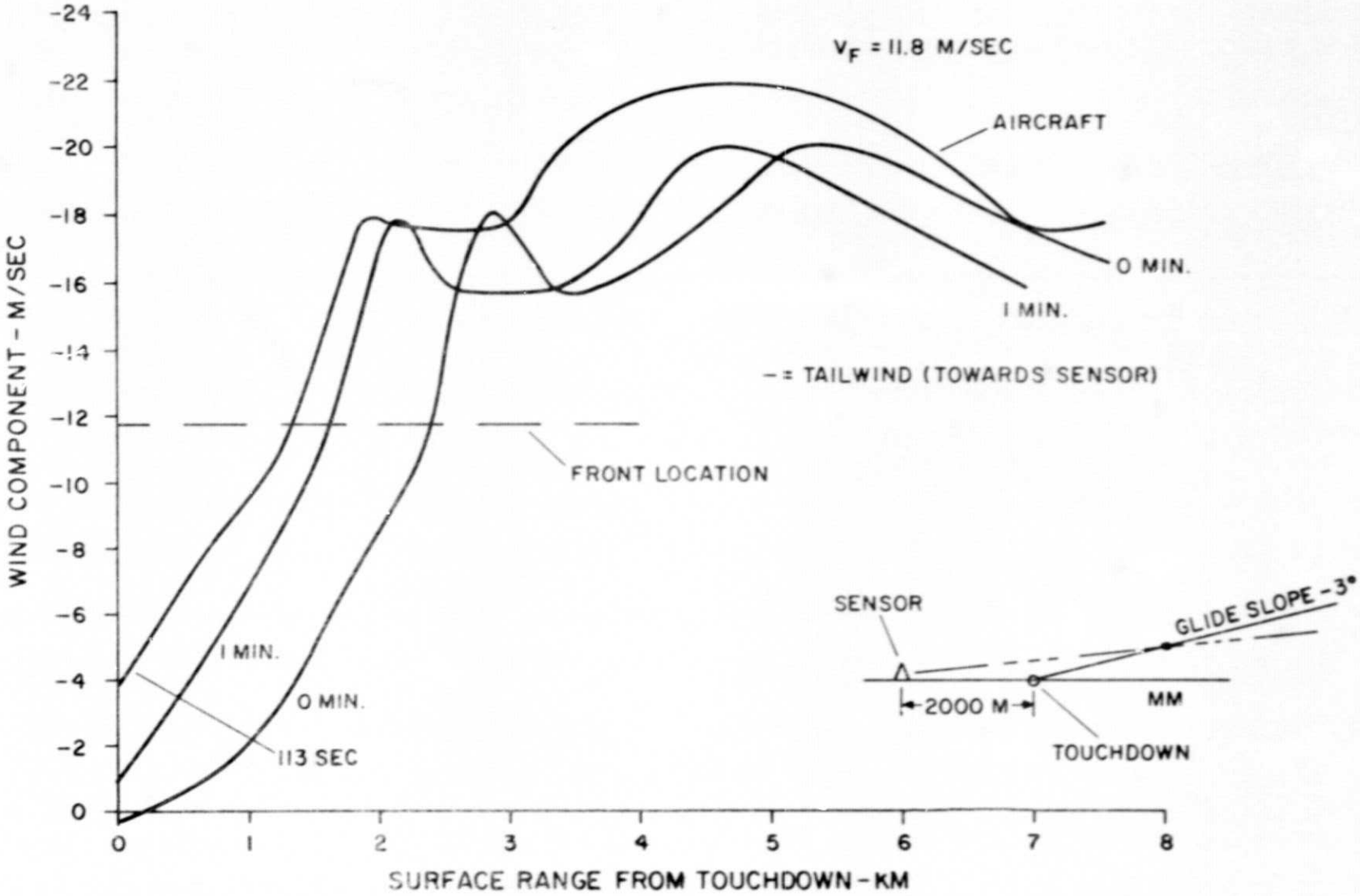

Figure 11. Comparison of Aircraft Experienced Wind and Touchdown Sensor Measurements

as the beam was scanned in azimuth. A significant difference between this wind field and that discussed earlier is that it is horizontally homogeneous and therefore is striated in horizontal layers not dissimilar to what might be expected from a thermal inversion and the shallow slope of a warm front. (Note in Figure 8 the bulge in horizontal wind at the 150 meter altitude region). This characteristic of the wind field causes significant changes in the measured Doppler as the sensor location is displaced.

Figure 12 depicts the Doppler wind field obtained when the LIDAR beam is scanned at an elevation of 3 degrees between ± 45 degrees in azimuth for a sensor at touchdown.

Figure 13 presents the same information for a sensor displaced from the touchdown location by 1524 meters in the down runway direction and, as indicated on the figure, scanned through a point on the glideslope directly above the middle marker. For compatibility with Figure 12 the sensor offset from touchdown (approximately 1524 m) was subtracted from the range magnitude and the range of azimuth angles was varied to encompass approximately the same physical area as depicted in Figure 12.

Comparing the two figures, the effects of the horizontally striated wind field causes the peak wind Doppler contour (12 m/sec) to occur at different ranges and to be stretched in range. If the atmosphere were truly homogeneous, this distortion could be processed out. As previously mentioned, in the atmospheric boundary layer, this is not often a correct assumption.

The difference between the two scans in terms of the wind Doppler they predict for an aircraft flying down the glide slope is shown in Figure 14. It is seen that the displaced sensor erroneously predicts the Doppler onset rate. This particular wind field, truly horizontally homogeneous, would be easily sensed by a conically scanned VAD type LIDAR system.

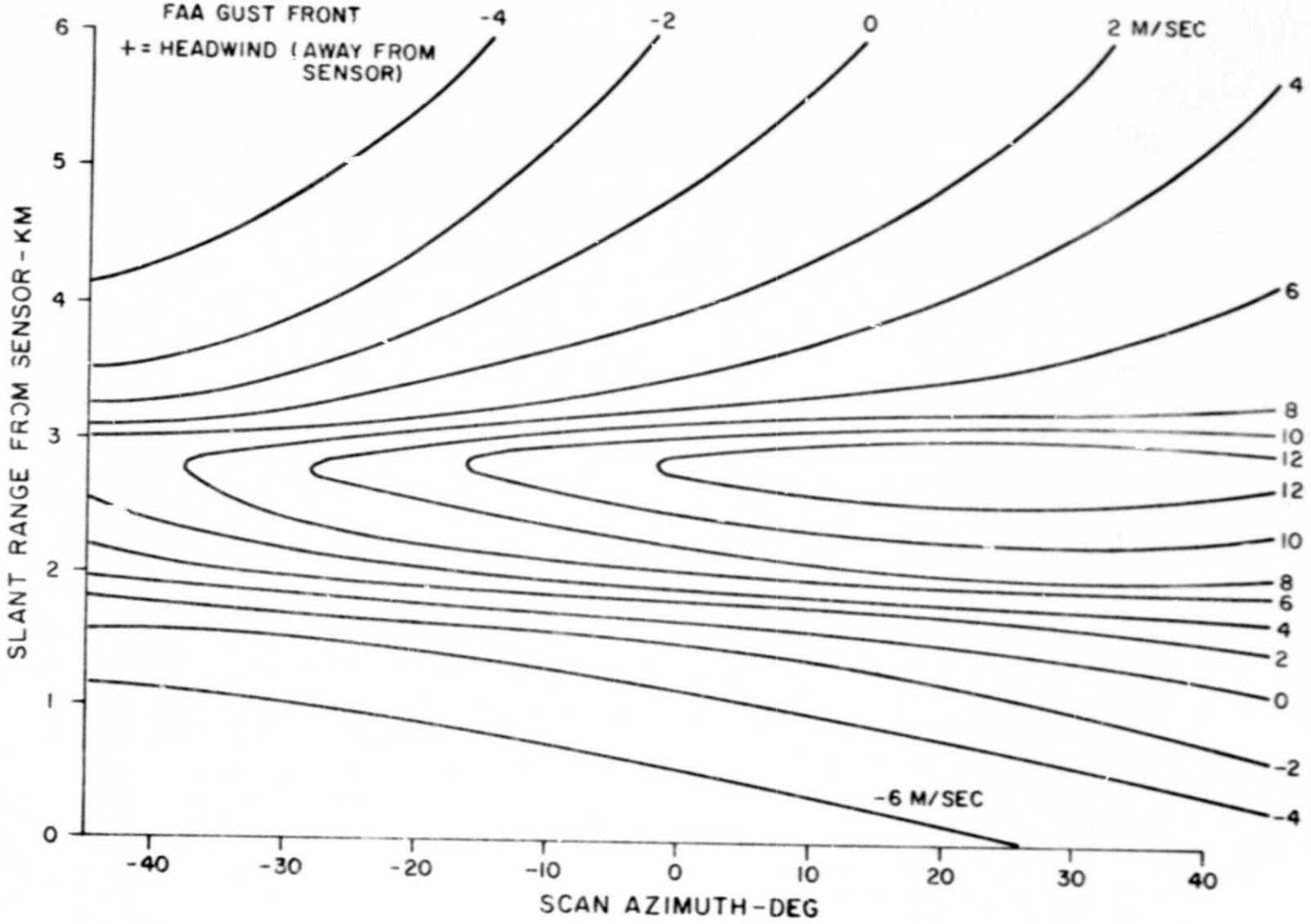

Figure 12. Doppler Wind Field Sensed by Azimuth Scanning Touchdown Sensor

RAYTHEON COMPANY
EQUIPMENT DIVISION
RAYTHEON

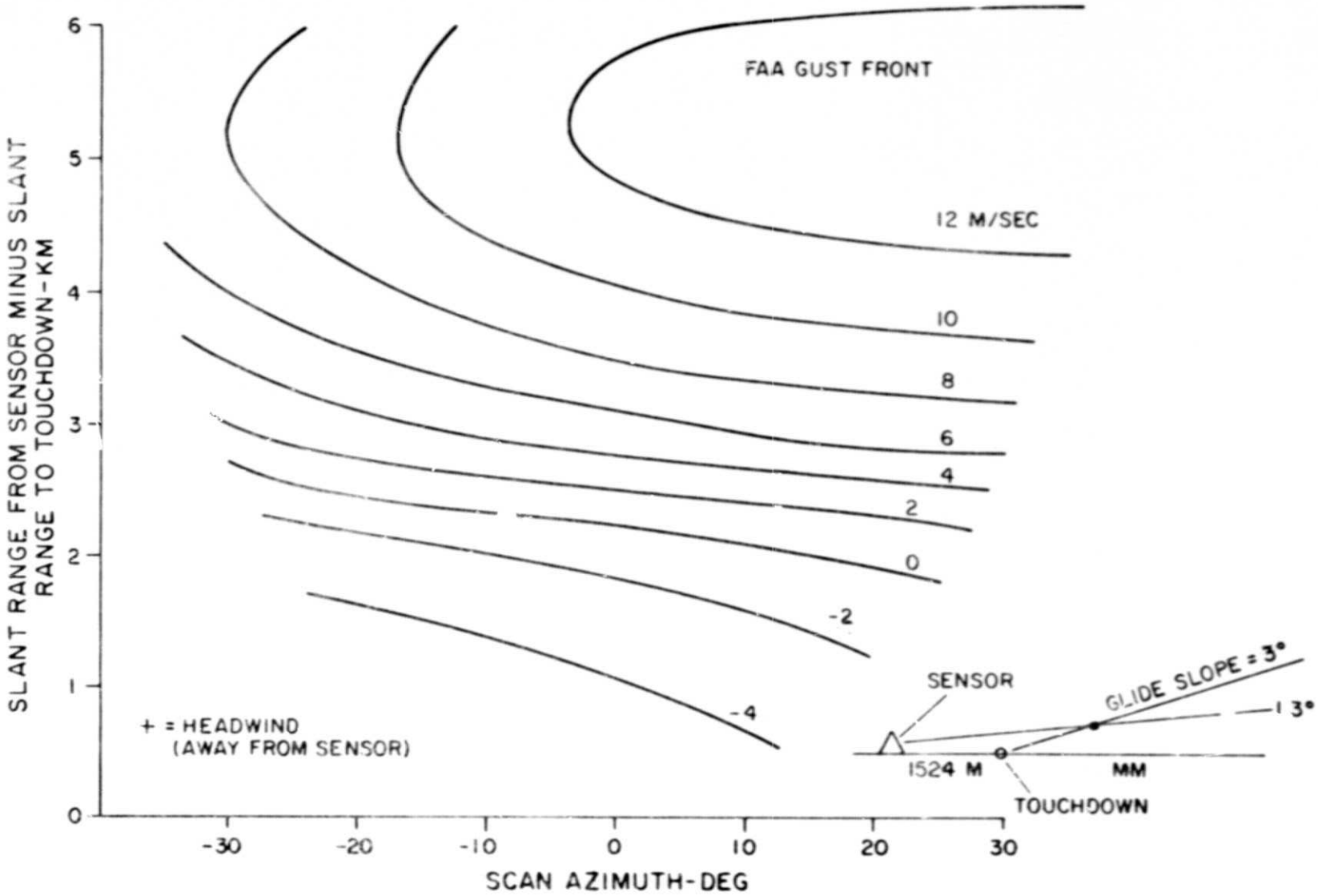

Figure 13. Doppler Wind Field Sensed by Azimuth Scanning Displaced Sensor

The possibility of utilizing an adaptive glideslope sensor consisting of a system normally directed up the glideslope, but periodically scanned in azimuth was also examined. The primary mission of the adaptive system would be to provide detail wind-shear information along the approach path but a secondary capability of warning of the approach of frontal systems from the side would also be provided.

The adaptive glideslope system would be located just off the runway at the runway midpoint. At this location both ends of the runway could be scanned depending on the direction of use. The nominal scan elevation angle would be directed to intersect the glideslope at some nominal range similar to the sketch shown on Figure 13.

The feasibility of an adaptive system depends upon the ability to collect lateral information while performing the main function of tracking the expected air speed changes along the approach path.

A typical scan history might provide a duty cycle of 80 percent, i.e. 80 percent of the time would be spent performing the primary mission of providing glideslope data and 20 percent would be spent in providing lateral (approaching windfield) information. During the lateral mode a uniform azimuth scan rate at a fixed elevation angle (perhaps the same angle as in the glideslope mode) would be utilized.

Figure 15 presents the maximum angular scan rate possible as a function of range for 12 inch and 18 inch aperture Lidars based on lag angle considerations. The maximum scan rate for a 12 inch aperture system is 25 deg/sec for a 10 kilometer range and 12.5 deg/sec for a 20 kilometer range. The time required to scan 360 degrees in azimuth is 14.4 seconds (10 km system). With an 80 percent duty cycle this amounts to 57.6 seconds for tracking along the

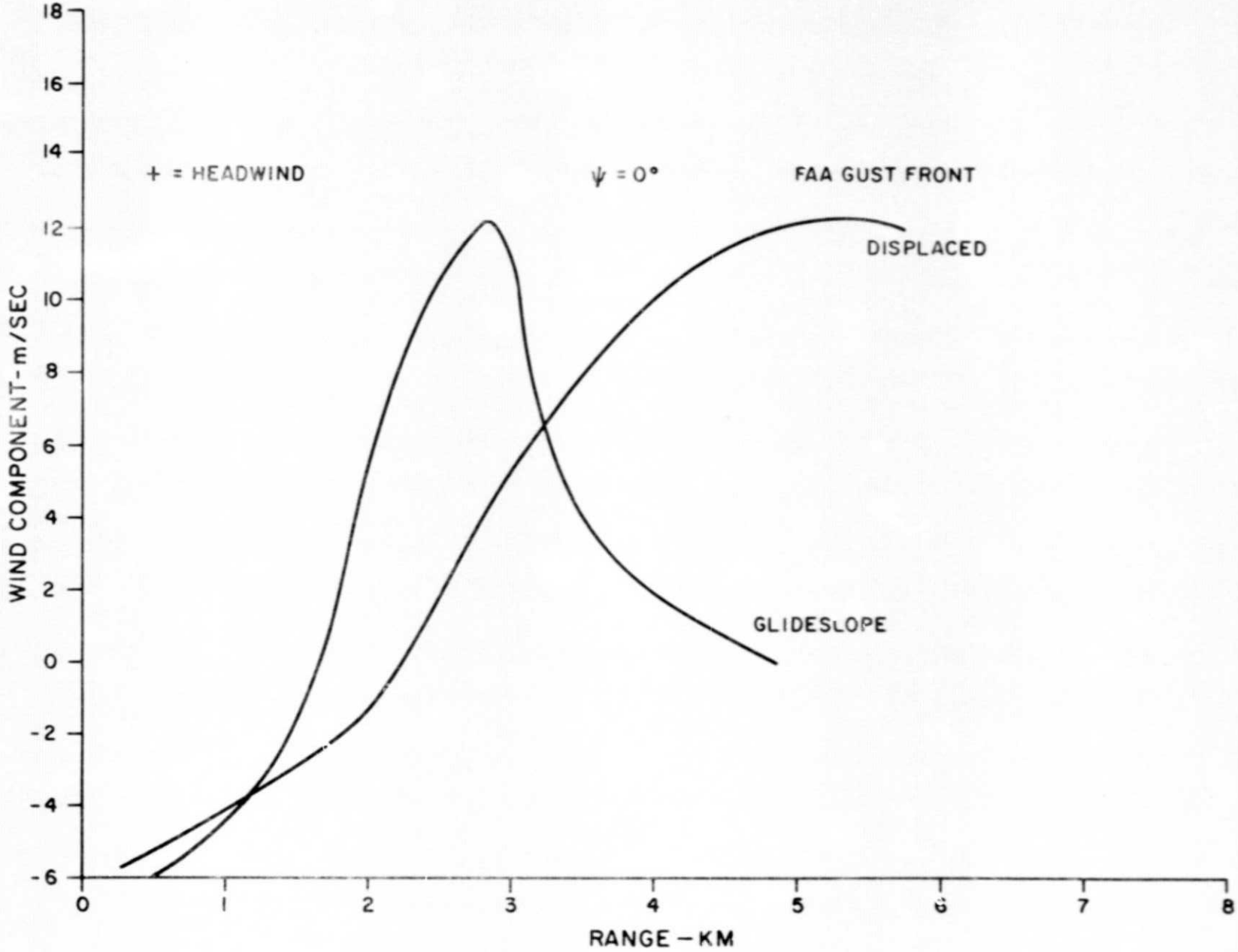

Figure 14. Doppler Wind Prediction of Two Sensors

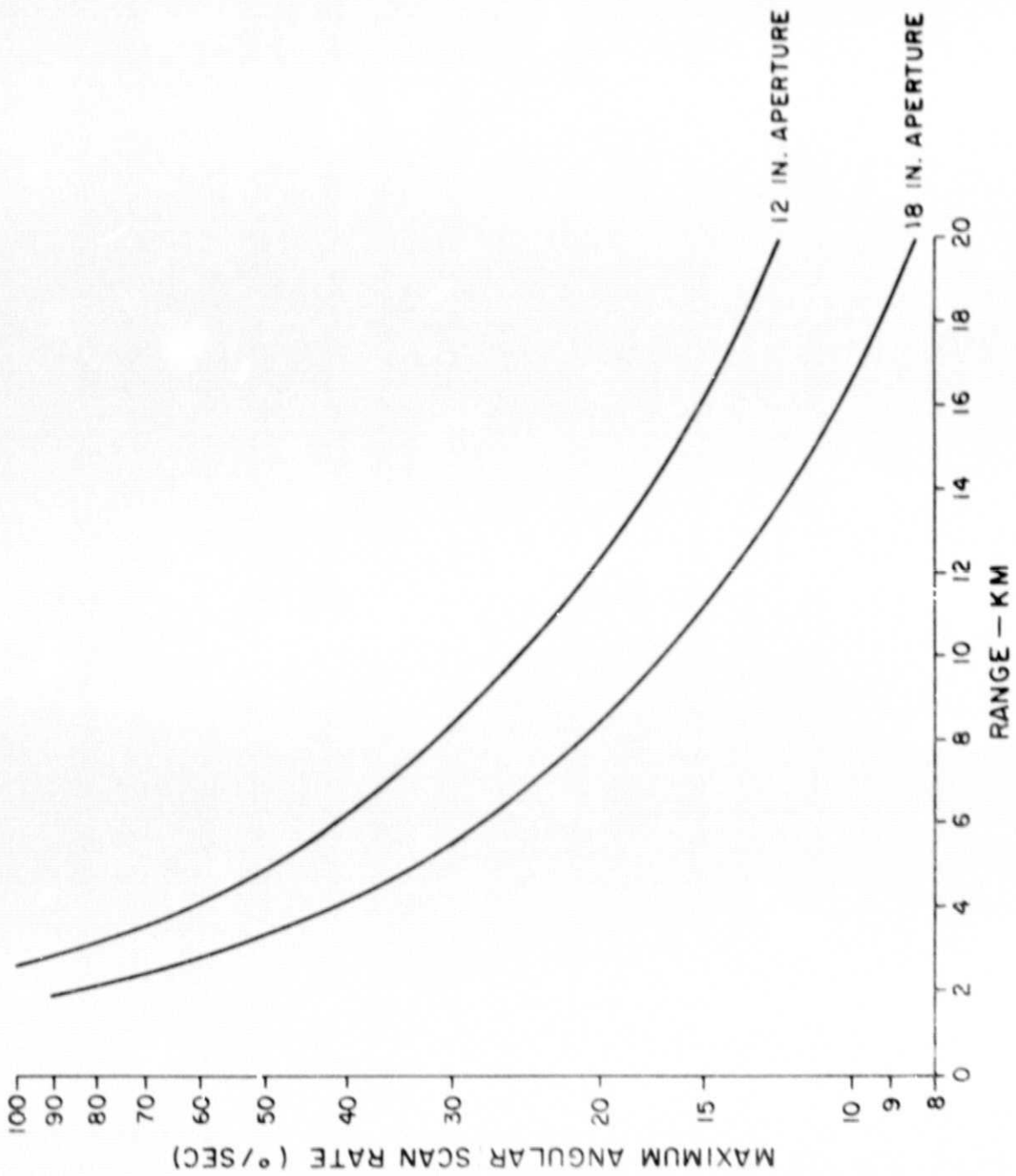

Figure 15. Maximum Scan Rates Limited By Lag Angle Losses (3 dB)

glideslope followed by a 14.4 second azimuth scan or a total time of 72 seconds. For a 20 km system, a total of 144 seconds is required with 28.8 being used for the aximuth scan. Table 2 lists the separation of sample points for various PRF values.

TABLE 2

Sample Separations
For Azimuthal Scan

PRF	Angular Separation (mrad)		Linear Separation (m)	
	10 km	20 km	10 km	20 km
200	2.3	4.6	23	92
100	4.7	9.4	47	188
50	9.3	18.6	93	372
20	23.3	46.6	233	932
10	46.6	93.2	466	1864

In order to predict the time of arrival of windshifts, frontal systems must be tracked as they approach. This requires at least three and preferably four looks at the frontal system during approach. Table 3 summarizes the number of looks possible as a function of the cross runway approach speed of the storm. Note, that the number of looks is independent of the sensor range due to a corresponding change in cycle time and maximum scan rate.

TABLE 3.

Number of Storm Observations

Storm Approach Speed (MPH)	Number of Looks (Scan Cycles)
10	30
20	15
30	10
40	7
60	5

Table 3 shows that even for storms that approach at high speed, the number of looks is adequate to track the storm during approach.

A drawback to the adaptive scan system is that it causes periodic interrupts to the windshear data along the approach path. Based on the data of Figures 7 and 8 which show the doppler windfield changes as a function of time and the previous analysis concerning lateral storm transport, the doppler windspeed versus range measured by the sensor is not expected to vary considerably during the 14.4 seconds spent performing the azimuth scan (10 km range case).

The adaptive scan system appears to be a reasonable approach to providing coverage to both ends of a runway while simultaneously providing warning of frontal wind shifts approaching from a cross runway direction. A system with a maximum range capability of 10 kilometers provides an adequate number of looks for frontal systems approaching even at high speeds. Other than providing improvement in velocity resolution, pulse repetition frequency increases from 20 Hz to 200 Hz are not expected to affect the results indicated.

7. CONCLUSIONS

A study of the application of a CAT type CO_2 pulse Doppler LIDAR as a wind shear sensor has been examined. The study has shown that the resolution characteristics of such a sensor operating at a pulse length of 2 μs are reasonably compatible with the minimum wind shear gust measuring requirements predicted by available data. Such a sensor could be applied to general wind field Doppler surveillance by locating the sensor at the airport center and scanning in azimuth out to maximum range. Adequate update capability is available with a 12" aperture system. At a maximum range of 10 km the system can update every 14 seconds, thus allowing the tracking of wind shear storms through the airport area.

Other deployment alternatives include providing glide slope wind Doppler information. In this case, the present CAT sensor must be displaced from the touchdown location by the minimum range capability of the system (approximately 2250 meters). Data from such a system would be in excellent agreement with actual aircraft experienced Doppler provided the wind field is vertically striated. In a horizontally striated wind field the glide slope sensor could be used, but would have to be scanned in elevation and range to obtain wind Doppler data along the actual glideslope. It should be noted that in cases of horizontally homogeneous wind fields (low level inversion and most warm fronts) the CW CO_2 Doppler LIDAR is also a viable sensor. Future application of the pure glideslope sensor could lead to fully automated landing capability where the feedback of the LIDAR obtained wind Doppler could be used in real time for insertion into the autopilot/autoland system. The latter could provide near all weather capability and therefore only one runway (both ends) might be instrumented to service an entire airport thereby reducing the system cost.

8. REFERENCES

(1) NTSB-AAR-74-14

(2) NTSB-AAR-76-B

(3) NTSB-AAR-76-14

(4) Fichtl, George H., Wind Shear Near the Ground and Aircraft Operations J. of Aircraft, Vol. 9, No. 11, November 1972.

(5) Barr, N. M. et al, Wind Models for Flight Simulation Certification of Landing and Approach Guidance and Control System, Report No. FAA-RD-74-206, December 1974.

(6) Goff, R. W., Thunderstorm-Outflow Kinematics and Dynamics, NOAA TM ERL NSSL-75, December 1975.